






Open Archive Toulouse Archive Ouverte (OATAO)

OATAO is an open access repository that collects the work of Toulouse researchers and makes it freely available over the web where possible

This is an author's version published in: <http://oatao.univ-toulouse.fr/24508>

Official URL: <https://doi.org/10.1002/sia.6606>

To cite this version:

Giffard, Kévin  and Arurault, Laurent  and Blanc, Christine  and Di Caprio, Dung *Accurate evaluations of both porosity and tortuosity of anodic films grown on rolled AA 1050 and on rolled or machined AA 2024 T3.* (2018) *Surface and Interface Analysis*. 1-10. ISSN 0142-2421

Any correspondence concerning this service should be sent to the repository administrator: tech-oatao@listes-diff.inp-toulouse.fr

Accurate evaluations of both porosity and tortuosity of anodic films grown on rolled AA 1050 and on rolled or machined AA 2024 T3

Kévin Giffard^{1,2} | Laurent Arurault²  | Christine Blanc³ | Dung Di Caprio⁴

¹MECAPROTEC Industries, Muret, France

²CIRIMAT, Université de Toulouse, CNRS, UT3 Paul Sabatier, Toulouse Cedex 9, France

³CIRIMAT, Université de Toulouse, CNRS, ENSIACET, Toulouse Cedex 4, France

⁴Chimie Paristech, Institut de Recherche de Chimie Paris (IRCP), PSL Research University, CNRS, Paris, France

Correspondence

Laurent Arurault, CIRIMAT, Université de Toulouse, CNRS, Université Toulouse III, 118 Route de Narbonne, 31062 Toulouse Cedex 9, France.

Email: arurault@chimie.ups-tlse.fr

Funding information

European Union (ERDF); French Ministry of Industry (DIRECCTE); Midi-Pyrénées Region; MECAPROTEC Industries; Association Nationale de la Recherche et de la Technologie (ANRT), Grant/Award Number: CIFRE n°2011/1617

The porosity of the anodic films grown on aluminium substrates depends on various operating conditions related to the anodization electrolyte and to the applied electrical parameters, as well as to the substrate itself. In the present study, three different aluminium substrates were studied and anodized: AA 1050 (rolled; thickness = 1 mm), AA 2024 T3 (rolled; 1 mm), and AA 2024 T3 (machined; 3 mm). For each type of anodic film, the porosity, as well as its changes during anodization, was accurately characterized using both field-emission gun scanning electron microscopy (FEG-SEM) and a reanodization technique. Moreover, for the first time, the corresponding tortuosity was quantified for all studied substrates. Results for rolled AA 2024 T3 and for machined AA 2024 T3 especially showed significant differences in tortuosity values, contributing towards clarifying, in part, their different wettability characteristics or anticorrosion behaviour, so far not clearly explained.

KEYWORDS

aluminium alloys, anodic films, anodization, porosity, tortuosity

1 | INTRODUCTION

Various authors have studied the morphological characteristics of porous anodic films formed on pure metals¹⁻⁵ or alloys.⁶⁻⁸ The porosity of the anodic films grown on aluminium substrates depends on various operating conditions, related to the anodization electrolyte and to the applied electrical parameters, as well as the substrate itself. Pure substrates thus allow anodic aluminium oxide (AAO) templates with highly ordered porosities⁹⁻¹² to be produced; these latter have been extensively studied.^{13,14} In contrast, complex and tortuous porosities are usually obtained for multiphase aluminium alloys, eg, aeronautical AA 2XXX or 7XXX.^{15,16}

Electronic imaging (field-emission gun scanning electron microscopy [FEG-SEM] or MET) generally remains the main characterization technique to evaluate the microstructure of the anodic films, ie, mainly the average pore diameter and consequently the porosity.¹⁷ However, this technique has major limitations relating to resolution of the image, accuracy of the analysis software, and also the representativeness of porosity (through 2D images). The aim of the present study is to accurately evaluate the porosity and, for the first time, the tortuosity

of the anodic films prepared on a relatively pure aluminium substrate (ie, rolled AA 1050 showing thickness of 1 mm) and on multiphase substrates, ie, rolled AA 2024 T3 (1 mm) and machined AA 2024 T3 (3 mm). Three different techniques (FEG-SEM, reanodization, and Brunauer-Emmett-Teller [BET]) were used, and the results were compared. The final perspective relates to detecting any differences in porosity-tortuosity between films prepared on rolled or machined AA 2024.

2 | EXPERIMENTAL

1050A aluminium alloy (99.5% Al, <0.40% Fe, <0.25% Si, and <0.05% Cu, wt%) and 2024 T3 alloys (90.7 < Al < 94.7%, <0.50% Fe, <0.50% Si, 3.8 < Cu < 4.9%, 1.2 < Mg < 1.8%, 0.3 < Mn < 0.9%, <0.25% Zn, <0.15% Ti, 0.10% Cr, wt%) were both used, as three different types of substrates: 1050 (rolled; thickness = 1 mm), 2024 T3 (rolled; 1 mm), and 2024 T3 (machined; 3 mm). Moreover, all chemical compounds used were analytical grade, while aqueous electrolyte solutions were obtained using deionised water.

2.1 | Surface preparation

The preparation process^{18,19} mainly involved three successive steps: degreasing, etching, and finally anodization.

An aluminium alloy sheet (50 × 50 × 1 mm of treated surface) was degreased firstly by acetone (CH₃)₂CO and secondly for 20 minutes in an aqueous bath (pH ≈ 9; 60 ± 2°C) containing sodium tripolyphosphate Na₅P₃O₁₀ (40 g L⁻¹) and sodium tetraborate (borax) Na₂B₄O₇·10H₂O (40 g L⁻¹) and then etched in aqueous sulphoferric solution (pH ≈ 2; 25 ± 5°C) for 5 minutes. The samples were immediately rinsed at ambient temperature with distilled water after each step.

The sample was then used as an anode and a lead plate (56 × 56 × 1 mm of immersed surface) as a counter electrode in an electrochemical cell, containing an aqueous H₂SO₄ stirred bath (200 rpm; 200 g L⁻¹, ie, 2.039 mol L⁻¹), thermostated using a Huber CC2 cryostat at 19.0 ± 0.5°C and 20.0 ± 0.5°C for AA1050 and AA2024, respectively. The anodization was run in potentiodynamic mode²⁰ with an initial voltage ramp (0.05 V s⁻¹, 0-16 V, 320 s) and voltage plateau at 16 V. The total duration was adapted to each alloy (920 s for AA1050 and 1220 s for AA 2024) so as to obtain a resulting film thickness typically equal to 5.0 ± 0.5 μm.

2.2 | Characterizations

FEG-SEM (JEOL JSM 6700F) was used to observe the porous anodic film, while ImageJ free software was used to analyse the SEM images and then evaluate the film's characteristics, ie, the pore density (ρ_{pores}), the pore average diameter (d_{pore}) from the FEG-SEM surface views, the height of the porous layer (h_p), and the thickness of the barrier (or compact) layer (h_b) from the cross-sectional views. Porosity (or void percentage) (τ_{FEG}) stemming from the FEG-SEM views was thus calculated:

$$\tau = \rho_{\text{pores}} \cdot \pi \frac{d_{\text{pore}}^2}{4}. \quad (1)$$

The mercury porosimetry method,²¹⁻²³ which usually allows the pore diameter distributions in porous materials to be determined, could not be performed successfully here. Indeed, this method is not suitable in the case of anodic films supported on aluminium substrates since, on the one hand, mercury and aluminium can form an amalgam²⁴ and, on the other, the pressures applied can damage the film walls during such measurements.

The pore surface of the final anodic films was measured with krypton gas by BET method using an ASAP 2010 Micromeritics device. The measuring chamber, containing 20 cm² of plates anodized on one side, was previously degassed at a temperature of 110°C and a pressure of 10⁻² Pa for 12 hours. In this case, the specific surface is not expressed in m² g⁻¹ for two reasons. The first lies in the fact that during BET measurement, the anodic film is always supported on the substrate, while the second is based on the difficulty of precisely determining the mass of the anodic film due to its complex composition, ie, in fact a mixture of hydrated Al₂O₃, Al(O)OH, and Al(OH)₃, with inclusions of elements coming from the aluminium alloy and anions from the electrolyte.²⁵ The surface obtained by BET analysis (S_{BET}) will therefore be expressed per unit of geometrical surface of film (m² cm⁻²) and not m² g⁻¹.

A third technique known as "reanodization" (or also the "Dekker-Van Geel" technique)²⁶⁻³² was used; this is based on a second galvanostatic anodization (also called the "forming" step) of a first porous anodic film, in a mixed boric acid-tetraborate electrolyte (H₃BO₃ 0.5 mol L⁻¹; Na₂B₄O₇ 0.05 mol L⁻¹).^{28,30,32} At a constant forming current density (here J = 0.5 mA cm⁻²),^{28,32} the voltage increases linearly with the gradual filling of the porosity, which results when the filling is integral with a slope break (from m₁ to m₂), also called the "knee voltage," at time t_p (Figure 1). Experimentally, this knee voltage is not usually a well-defined slope change but rather a smooth change.³⁰ The slope then decreases (m₂ < m₁) since the growth rate drops, with the porosity (τ_{forming}) changing from an α value (0 < α < 1) in the porous film to 1 above the filled film. It is then possible to determine the porosity (τ_{forming}) using the following formula^{28,30,32}:

$$\tau_{\text{forming}} = \frac{T_{\text{Al}^{3+}} \cdot \left(\frac{m_2}{m_1}\right)}{1 - (1 - T_{\text{Al}^{3+}}) \left(\frac{m_2}{m_1}\right)}, \quad (2)$$

where T_{Al³⁺} is the transport number of Al³⁺ ions, assumed to be equal³⁰ to 0.4.

3 | RESULTS AND DISCUSSION

3.1 | Characteristics of the final anodic films

At the end of the first anodization, the thickness of the anodic films was 5.0 ± 0.5 μm, regardless of the substrates used. The porosity of the anodic films prepared on rolled AA 1050 and 2024 (1 mm) and on machined AA 2024 (3 mm) was then observed through FEG-SEM

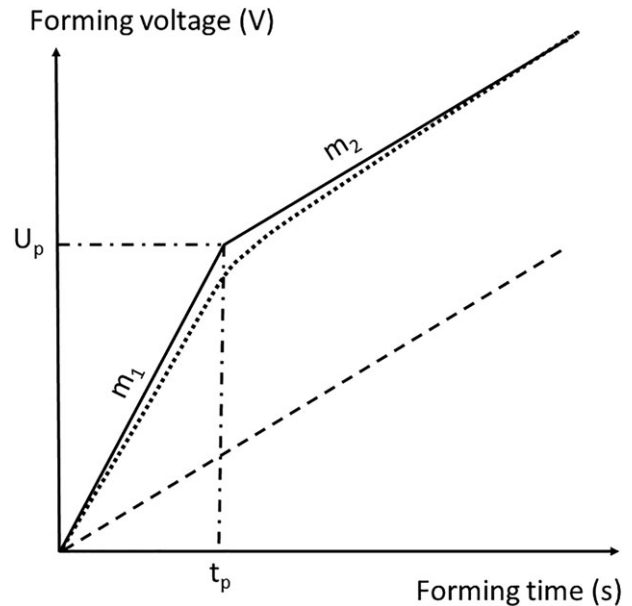


FIGURE 1 Voltage versus forming time plot during reanodization of an ideal porous anodic film prepared on a smooth aluminium substrate. The dotted line is a typical experimental reanodization curve obtained on an anodic film on rough aluminium substrate, while the dashed line corresponds to the barrier anodization of a nonanodized aluminium substrate

surface views (Figure 2). ImageJ analysis of these images provided the morphological characteristics (pore diameters and pore density) of the anodic films. Figure 3 shows in particular the distributions of pore diameters in relation to the substrate used.

The anodic film on AA 1050, showing a main pore diameter in the 6 to 18 nm range (Figure 3A), has a slightly larger pore size distribution than both films supported on AA 2024 (Figure 3B,C); the pore diameters for these films are ranging from 4 to 14 nm.

Table 1 shows the average pore diameters and pore density, as also as the resulting porosity for each of the anodic films. The average pore diameter for film on AA 1050 is 10 ± 4 nm, while the films on both AA 2024 (1 and 3 mm) have an average pore diameter of 8 ± 2 nm. However, considering the standard deviations, these average diameters cannot be considered to be significantly different.

Table 1 also shows that the pore densities of the films ($2.5 \cdot 10^{11}$ and $3.2 \cdot 10^{11}$ pores per cm^2) prepared on both AA 2024 substrates (rolled and machined, respectively) seem to be greater than that ($1.8 \cdot 10^{11}$ pores per cm^2) of the anodic film on AA 1050. However, whatever the substrate considered, the porosity seems finally to remain unchanged, having a value from 15 to $17 \pm 3\%$. To summarize, the FEG-SEM surface views and their subsequent analyses thus appear to show comparable final porosity for the anodic films prepared on the three types of substrates. This result should be put into perspective considering that either the porosities are effectively equivalent or that this experimental approach (based on FEG-SEM surface observations) may not be sufficiently effective to evaluate the characteristics (especially the porosity) of these anodic films.

TABLE 1 Characteristics (based on FEG-SEM views) of final anodic films prepared on (1) rolled AA 1050, (2) rolled AA 2024 T3, and (3) machined AA 2024 T3

	Rolled AA1050	Rolled AA2024	Machined AA2024
Main pore diameter, nm	10 ± 4	8 ± 2	8 ± 2
Pore density, number per cm^2	$1.8 \cdot 10^{11}$	$2.5 \cdot 10^{11}$	$3.2 \cdot 10^{11}$
Porosity τ_{FEG} , %	15 ± 3	15 ± 3	17 ± 3

3.2 | Changes of the anodic film characteristics during the first anodization

It would appear interesting to evaluate the porosity changes during the growth of the anodic film, since the porosity may evolve, especially during the voltage ramp (0.05 V s^{-1} , 0-16 V, 0-320 s). The potential change in porosity was thus studied through two independent methods, ie, the FEG-SEM method and then the reanodization method.

3.2.1 | Study by microscopy of the anodic films on AA 1050

FEG-SEM surface and cross-sectional views were taken on anodic films prepared on AA1050 for different anodization times during the voltage slope (from 0 to 320 s) and the voltage plateau (from 320 to 380 s). From cross-sectional FEG-SEM views, the thickness of the anodic film (Figure 4) and the thickness of the barrier layer (Figure 5) were first determined. Figure 4 shows in particular that the film thickness changes little (slope 1) at the beginning of the voltage ramp (from

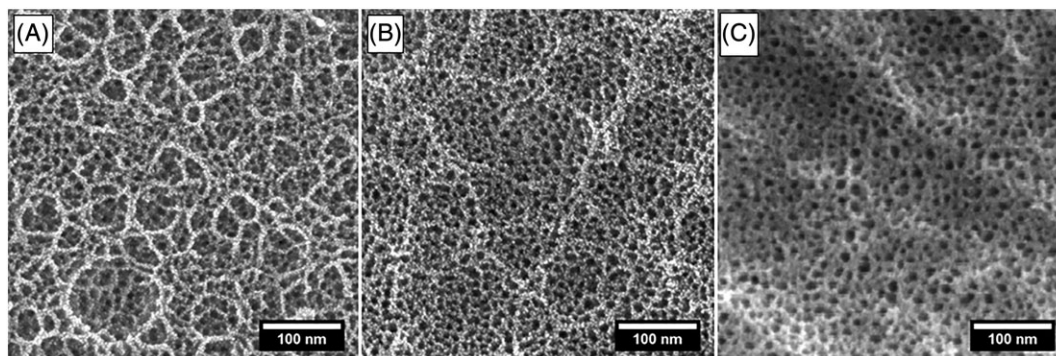


FIGURE 2 FEG-SEM surface views of the final anodic films prepared on A, rolled AA 1050 (1 mm), B, rolled AA 2024 T3 (1 mm), and C, machined AA 2024 T3 (3 mm)

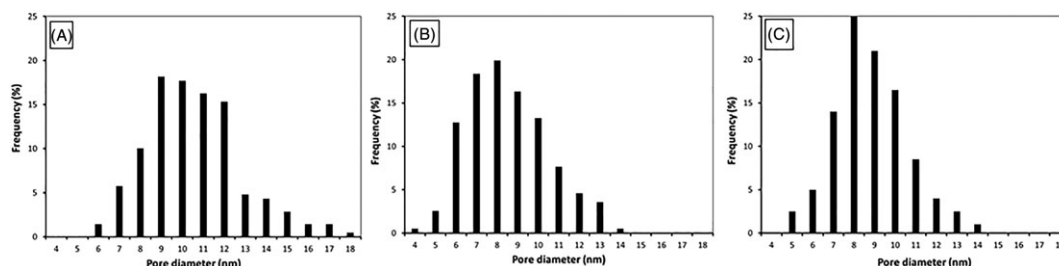


FIGURE 3 Distribution diagram of pore diameter of final anodic films prepared on A, rolled AA 1050, B, rolled AA 2024 T3, and C, machined AA 2024 T3

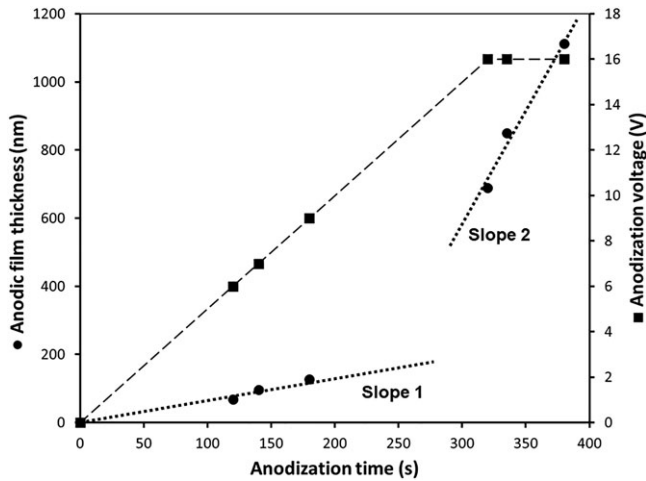


FIGURE 4 Anodic film thickness as a function of the anodization time and voltage on rolled AA 1050

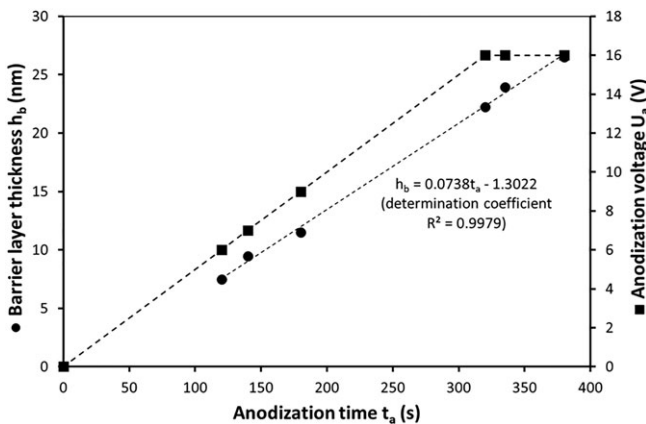


FIGURE 5 Barrier layer thickness as a function of the anodization time and voltage on rolled AA 1050

0 to 320 s, ie, from 0 to 16 V), whereas it increases significantly (slope 2), especially during the steady state, ie, after 320 seconds, for a voltage value at 16 V. In contrast, the thickness of the barrier layer regularly increases (slope 3) both during the transient regime (the voltage ramp) and during the steady-state voltage regime (Figure 5), in agreement with previous works.²⁹

In addition, FEG-SEM surface views provide the average pore diameter (Figure 6) and the average porosity of the anodic film (Figure 7) as a function of the anodization time. The pore diameter first increases considerably (from 0.0 to 7.1 nm after 140 s) and then increases from 7.3 (at 320 s) to 7.6 nm (at 380 s) at the beginning of the voltage plateau, reaching 10 nm for the 5 μm final film. The average porosity based on the FEG-SEM observations decreases slightly for the lowest anodization times (20-60s) (Figure 7) and then varies from 12.5% to 23.5% as the time increases from 60 to 380 seconds.

3.2.2 | Study by reanodization of the anodic films on AA 1050

Figure 8 clearly attests to the effective pore filling, as a function of the forming time, of an anodic film initially anodized for 320 s. Figure 8

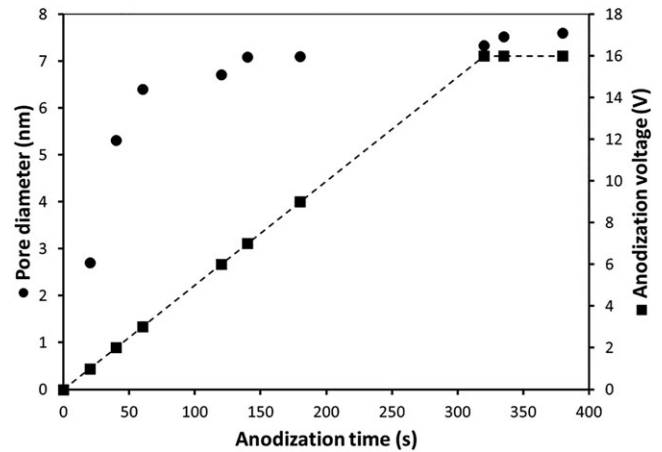


FIGURE 6 Average pore diameter (of the film prepared on rolled AA 1050) as a function of the anodization time and voltage

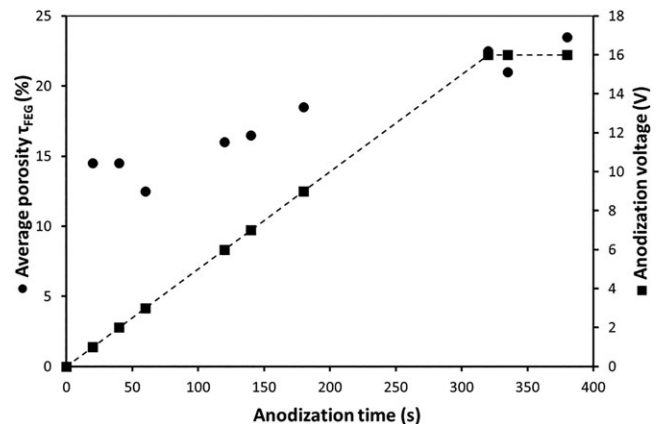


FIGURE 7 Porosity τ_{FEG} (of films prepared on rolled AA 1050) as a function of the anodization time and voltage

highlights the fact that the lower part of the film has a higher density since the pores are filled. The progressive pore filling with the reanodizing time is clearly visible, the filling being effective from the bottom to the top of the anodic film.

Figure 9 shows the voltage as a function of the forming time (0-400 s) for anodic films previously prepared on AA 1050 over different durations (20-180 s), ie, also different voltages (1-9 V). The starting voltages ($U_{t=0}$) are nonzero and gradually increase with the duration of the first anodization. Figure 10 shows that the starting voltage is in fact proportional to the first anodization duration. On the basis of the previous FEG-SEM observations (Figure 5), our results confirm that the starting voltage also depends on the thickness of the barrier layer of the original anodic film,²⁷ ie, also showing an increase with the ramp time (0-320 s) of the first anodization.

The first forming slope (m_1) corresponds to the filling rate of the film pores. The reanodization slope (m_1) thus becomes steeper for films having increasing durations of the first anodization (Figure 11). Otherwise, m_1 values seem proportional to the square root of the anodization voltage (Figure 12), as proposed previously.²⁹

Slope m_2 depicts the growth speed of the oxide above the filled anodic film, once the pores are completely occluded. The value of

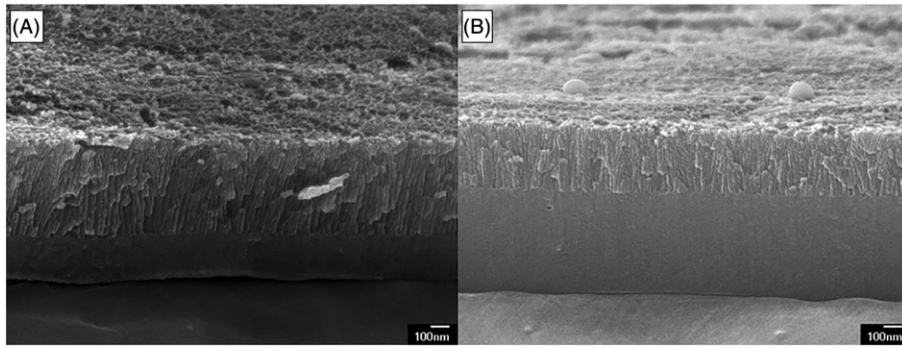


FIGURE 8 FEG-SEM cross-sectional views of anodic films prepared for 320 seconds and then reanodized for A, 330 and B, 950 seconds

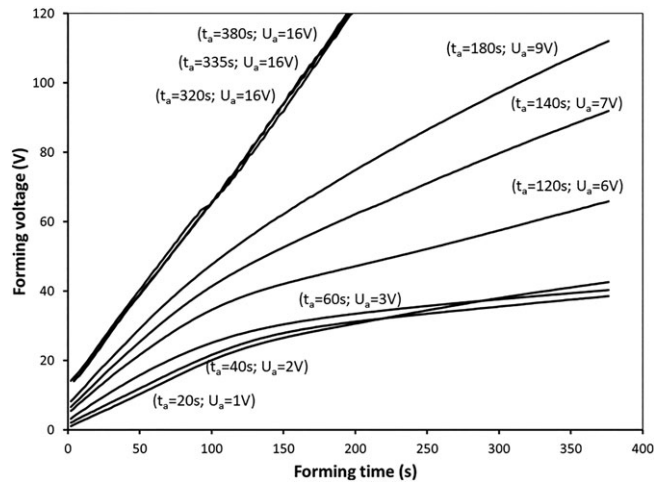


FIGURE 9 Forming voltage as a function of forming time for anodic films prepared on rolled AA1050 at different anodization durations (20-180 s)

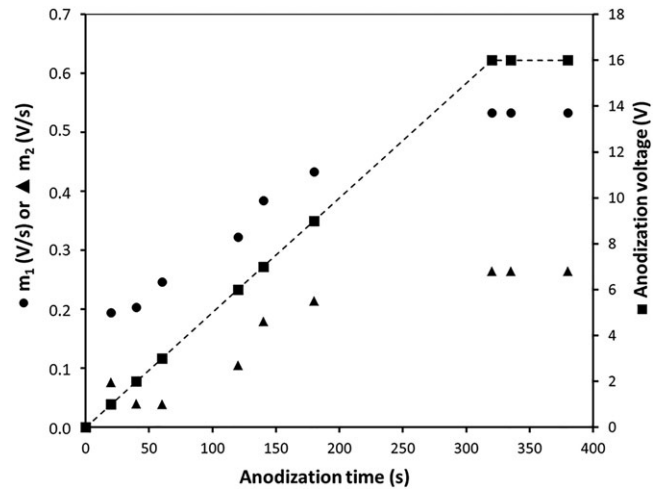


FIGURE 11 Slopes m_1 and m_2 as a function of the anodization time on rolled AA 1050

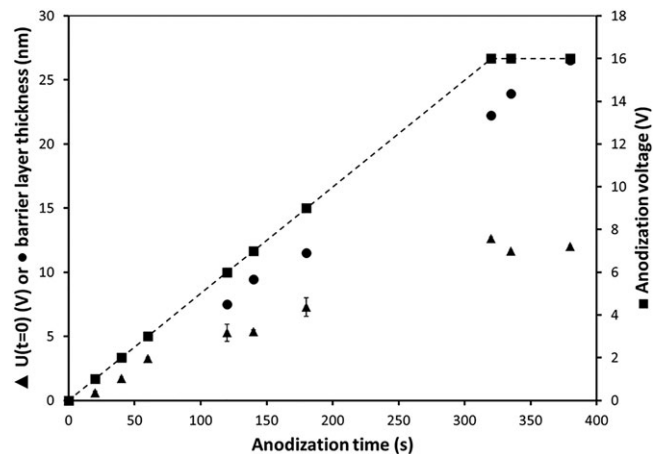


FIGURE 10 $U_{t=0}$ and barrier layer thickness as a function of anodization time on rolled AA 1050

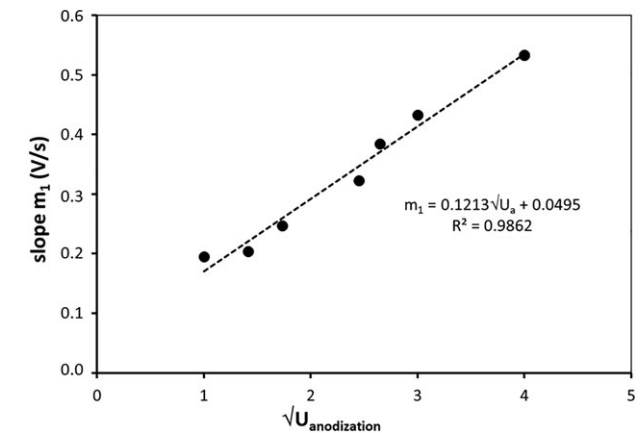


FIGURE 12 Slope m_1 as a function of the square root of the anodization voltage, on rolled AA 1050

m_2 decreases, in all cases, compared with m_1 (Figure 11) since the area of the barrier layer-solution interface increases. However, surprisingly, m_2 values are not identical for each anodic film and change with the anodization time, unlike in the findings of Takahashi²⁸ who showed that m_2 does not evolve for anodic films made with current densities between 0.5 and 5 mA cm⁻². Interface roughness could be an

explanation for this surprising result, considering that past works²⁸ usually performed the reanodization method on electropolished samples, while no (electro)polishing was used in this study.

Previous results correspond to the first anodization durations of less than 180 seconds, with the slope change (the knee voltage) being graphically determined from the forming curves (Figure 9). Meanwhile,

for the first anodization times greater than 320 seconds, the slope change is not observed since the film cannot be completely filled. In particular, complete pore filling is impossible from a reanodization time of 950 seconds, the electrical resistance being too high and electrical breakdown appearing on the surface of the film.³³⁻⁴⁰ Nevertheless, in this second case, porosity values can be extracted using the slope corresponding to the barrier layer formation on the pretreated and nonanodized AA 1050 substrate (Figure 13A). Indeed, the hypothesis, previously used by Ono et al,³² is to consider that the oxide growth on the nonanodized aluminium is similar to the growth above the thick films during reanodization. This hypothesis seems consistent insofar as the m_2 slope (0.2159 V s⁻¹) of the 180-second film is relatively close (Figure 13B) to the slope (0.2645 V s⁻¹) corresponding to compact film growth of the initially nonanodized substrate. Note also that finally, m_1 slopes (Figure 13B) of the films reanodized at 320, 335, and 380 seconds are superimposed, revealing that the porosity does not change when the plateau is reached that is to say from 320 seconds (ie, the nominal voltage value equals to 16 V).

The porosity (τ_{forming}) was then calculated from slopes (m_1 and m_2), using Equation 2 and assuming $T_{\text{Al}^{3+}}$ equal to 0.4²⁸; τ_{forming} main value is based on two experiments for each first anodization time. Figure 14 highlights a porosity decrease during the early stages of the first anodization, changing for instance from 20% for the film prepared for 20 seconds to 6% in the film anodized for 60 seconds. This porosity change is in agreement with Ono's work³² that reports such a porosity decrease with an increasing anodization voltage. In contrast, the porosity then increases from an anodization time of 60 seconds, finally stabilizing (at about 30%) at the voltage plateau. Our results therefore diverge from the previous proposed relation,^{29,30} suggesting a relationship between $(1/\tau_{\text{forming}})$ and $(\sqrt{V_{\text{anodization}}})$. This difference could be explained considering that previous works were conducted at constant anodization voltage, while the present study uses a voltage ramp in the 0 to 16 V range.

Figure 14 shows porosity values (τ_{FEG}), based on the FEG-SEM surface views, of the anodic films derived from the first anodization. These results are close to the porosity values obtained by the reanodization method in the 20 to 120 second time range. In contrast, for the first anodization time from 140 to 380 seconds, τ_{FEG} and τ_{forming} values are significantly different, τ_{FEG} being systematically

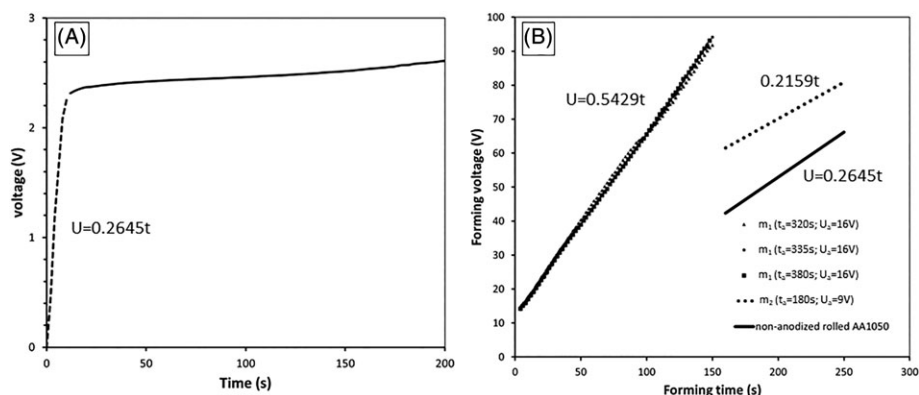


FIGURE 13 Forming voltage as a function of the forming time during A, the compact anodization of nonanodized rolled AA 1050 and B, the reanodization of AA 1050 anodized for 320, 335, and 380 seconds

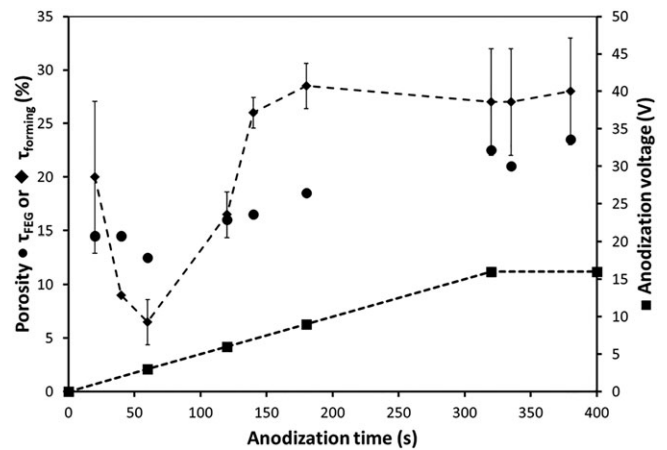


FIGURE 14 Porosities (τ_{forming} and τ_{FEG}) as a function of the anodization time and voltage

lower than τ_{forming} . This discrepancy supports the hypothesis that the film growth occurs at the substrate/barrier layer interface and consequently that the FEG-SEM surface observations correspond to the porosity created in the early stages of the first anodization.³²

3.2.3 | Study by reanodization of the anodic films on AA 2024

The same reanodization approach as adopted previously was then performed on an anodic film prepared over 380 seconds on AA rolled 2024 (1 mm). Figure 15 shows the forming voltage as a function of the forming time, while Figure 16 presents the corresponding FEG-SEM cross-sectional views. As the reanodization progresses, it appears that the film is not filled up from its bottom, as previously observed using AA 1050. On the contrary, growth of the oxide seems impeded, leading to the degradation of the film and the appearance of cavities at the substrate-film interface (Figure 16). This experimental phenomenon has not been reported in the literature, all previous works being performed only on pure aluminium substrates (usually higher than 99.5 wt%). Hitherto, no clear explanation has been given for this experimental observation, unless it be attributed to the tortuosity of the AA 2024 film pores. The present study is therefore further pursued with

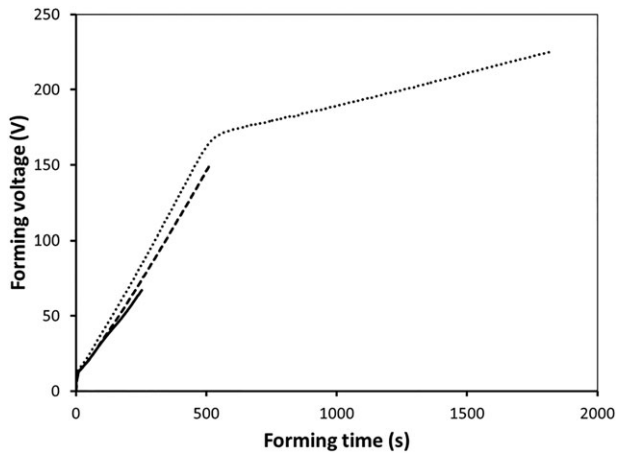


FIGURE 15 Forming voltage as a function of the forming time (5, 10, 30 min) on anodic films prepared (380 s) on rolled AA 2024 T3

the aim of evaluating another structural feature, tortuosity, which, to our knowledge, has not been studied for such anodic films.

3.3 | Evaluations of tortuosity

The anodic films were prepared on the three AA substrates (ie, rolled 1050 and rolled 2024 [1 mm] and machined 2024 [3 mm]), and then their respective cross-sections were observed by FEG-SEM (Figures 17 and 18). In particular, Figure 17 shows that, on the AA1050 substrate, the pores form columns arranged perpendicularly to the substrate at the

bottom of the film (Figure 17A). However, the pore orientation changes, and the pore organization becomes more complex at the top of the film (Figure 17B,C), reflecting a pore rearrangement during the increasing voltage ramp,⁴¹ ie, during the early stages of the first anodization.

Concerning the two other substrates on AA 2024 (1 and 3 mm), the anodic films both have a spongy structure with pores showing significant tortuosity (Figure 18). In the case of the anodic film on AA 2024 (1 mm), the tortuosity appears homogeneous over the entire thickness (Figure 18A-C). By contrast, the anodic film on machined AA 2024 (3 mm) seems to have a denser structure at the top than in the middle of the film (Figure 18E,F), the middle part being comparable with that observed on rolled AA 2024 (1 mm).

However, it is clear that these FEG-SEM observations remain partly subjective and qualitative, which motivated the use of another experimental approach, eg, based on the BET technique. This technique was implemented in order to first quantify the real specific surface (S_{BET}) of anodic films elaborated on the three substrates. In addition, the data from FEG-SEM surface analysis allowed a calculated specific area (S_{FEG}) to be obtained by assuming a cylindrical pores model and using Equations 3 and 4.

$$S_{FEG} = \rho \cdot S_{pore} + S_{ext} \quad (3)$$

$$\text{with } S_{pore} = 2 \pi \cdot R \cdot h_p + \pi \cdot R^2, \quad (4)$$

where S_{ext} is the area of the film top surface except the pores, h_p is the thickness of the anodic film, ρ is the pore density, S_{pore} is the surface of the pore walls, and R is the radius of the model cylindrical pore.

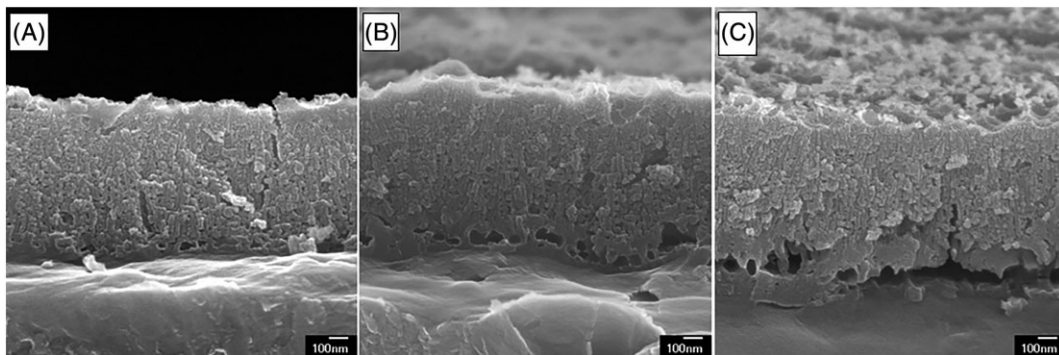


FIGURE 16 FEG-SEM cross-sectional views, as a function of the forming time (A, 5; B, 10; and C, 30 min), on anodic films prepared (380 s) on rolled AA 2024 T3

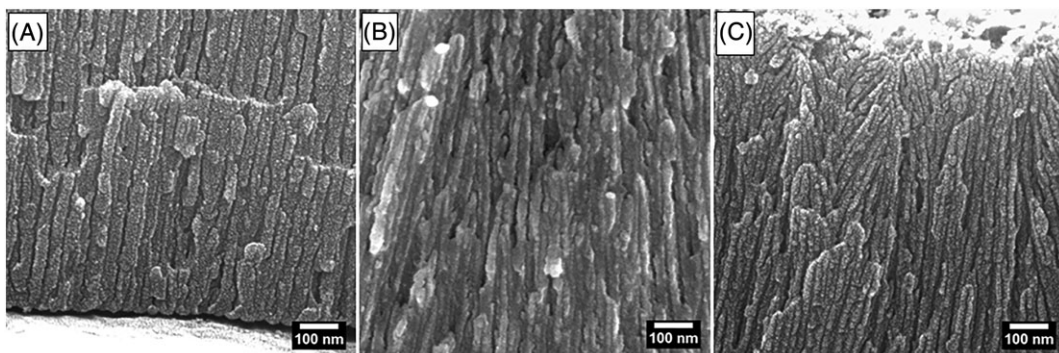


FIGURE 17 FEG-SEM cross-sectional views A, at the bottom, B, in the middle, and C, at the top of the final anodic film prepared on rolled AA 1050

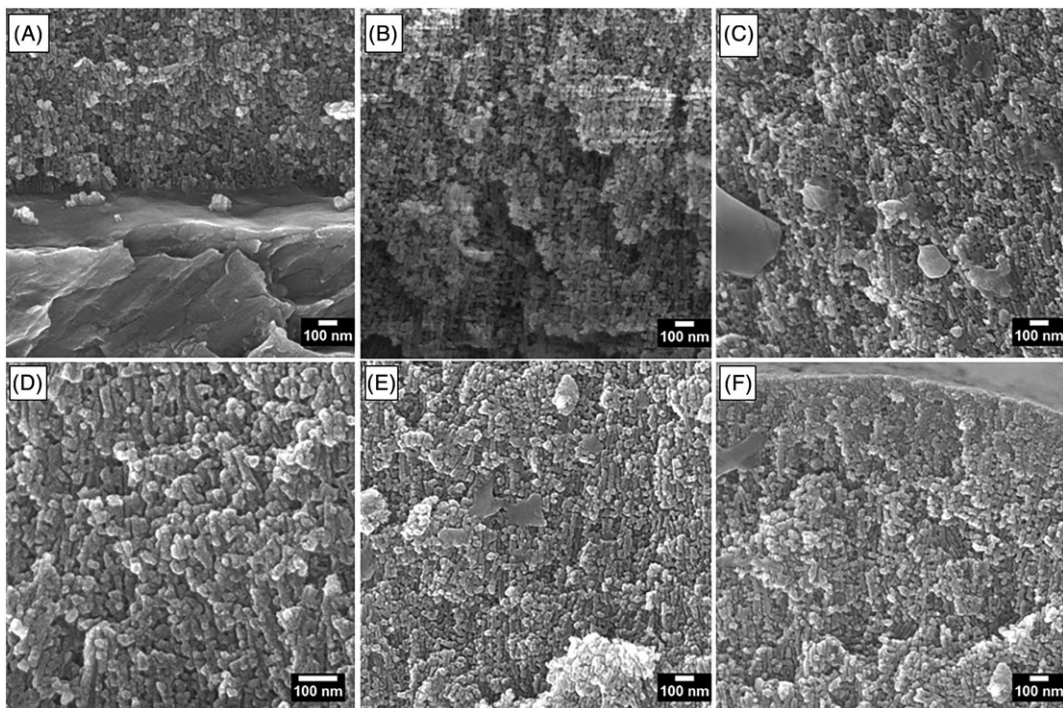


FIGURE 18 FEG-SEM cross-sectional views A, at the bottom, B, in the middle, C, at the top of the final anodic film prepared on rolled AA 2024 T3 (1 mm), and D, at the bottom, E, in the middle, and F, at the top of the final anodic film prepared on machined AA 2024 T3 (3 mm)

Table 2 then allows the specific surfaces measured by BET (S_{BET}) and those calculated using the model (S_{FEG}) to be compared for the three mean pore diameter values for each substrate. In the case of the AA 1050, the two specific surface values are close ($S_{\text{BET}} = 2.74$ and $S_{\text{FEG}} = 2.86 \text{ m}^2\text{-cm}^{-2}$) for a pore diameter of about 10 nm. In contrast, a significant difference was highlighted ($S_{\text{BET}} = 1.43 S_{\text{FEG}}$) in the case of the rolled AA 2024 substrate (1 mm). This difference was attributed to the tortuosity, whose contribution is not taken into account for the calculation of S_{FEG} , the pores being considered ideally cylindrical. The gap is further accentuated in the case of the machined AA 2024 (3 mm), which has a significantly higher BET surface area than the rolled AA 2024 (1 mm) (5.95 and $4.06 \cdot 10^{-2} \text{ m}^2 \text{ cm}^{-2}$, respectively). In fact, the surface calculated with the 8-nm pore diameter provided by the FEG-SEM data is equal to $3.62 \cdot 10^{-2} \text{ m}^2 \text{ cm}^{-2}$, this value being far from the value measured by BET ($5.95 \cdot 10^{-2} \text{ m}^2 \text{ cm}^{-2}$). Again, this difference is attributed to the tortuosity; Table 2 reports estimated values of the tortuosity for each of the three AA substrates,

ie, 0.96 (1050), 1.43 (2024 1 mm), and 1.64 (2024 3 mm). These results show in particular that this experimental approach would for the first time allow different types of porosity to be distinguished, in particular different spongy porosities. This approach is complementary to previous studies^{41,42} that focused on the evaluation of pore ordering degree and pore branching. The results also highlight the influence of forming steps of the substrate (here rolled AA 2024 [1 mm] or machined AA 2024 [3 mm]) on subsequent porosity of the anodic films, despite strictly identical surface treatments. These significant differences in tortuosity values could contribute to explaining the wettability changes on such porous anodic films.¹⁸

TABLE 2 Comparison of tortuosity and of the specific surfaces (measured S_{BET} and calculated S_{FEG}) of the final anodic films prepared on the AA substrates

	Rolled AA 1050	Rolled AA 2024	Machined AA 2024
$S_{\text{BET}} \cdot 10^{-2}, \text{m}^2 \text{ cm}^{-2}$	2.74 ± 0.02	4.06 ± 0.02	5.95 ± 0.02
Main pore diameter, nm	10 ± 4	8 ± 2	8 ± 2
Pore density (number per cm^2)	$1.8 \cdot 10^{11}$	$2.5 \cdot 10^{11}$	$3.2 \cdot 10^{11}$
$S_{\text{FEG}} \cdot 10^{-2}, \text{m}^2 \text{ cm}^{-2}$	2.86	2.83	3.62
Tortuosity	0.96	1.43	1.64

4 | CONCLUSION

Three different aluminium substrates (AA 1050 [rolled; 1 mm], AA 2024 T3 [rolled; 1 mm], and AA 2024 T3 [machined; 3 mm]) were studied and anodized in the same operating conditions, ie, electrolyte and applied voltage. For each type of anodic film, the porosity, as well as its changes during anodization, was accurately characterized using both FEG-SEM and the reanodization technique. Our results firstly confirm the limitations to determining porosity using FEG-SEM views; 2D surface views (ie, top interface of the anodic film) correspond in fact to pores formed at the early moments of the anodic film growth. Application of the reanodization approach then allows the porosity on anodic films prepared on AA1050 to be evaluated, showing in particular its complex change during the initial voltage ramp, before the steady-state voltage regime. Unfortunately, the reanodization technique appeared to be unsuitable for tortuous anodic films not prepared on pure aluminium like AA 1050 but on alloys such as AA2024T3. However, the corresponding tortuosity was successfully

quantified, for the first time, for all the studied substrates. Results thus showed significant differences in tortuosity values (0.96 [rolled AA 1050], 1.43 [rolled AA 2024], and 1.64 [machined AA 202]), contributing in part towards clarifying their different corrosion resistance characteristics or changes in wettability, as also the varying propensity of such porous anodic films to then be sealed.

ACKNOWLEDGEMENTS

Kévin Giffard thanks MECAPROTEC Industries and the Association Nationale de la Recherche et de la Technologie (ANRT) for his PhD grant (CIFRE n°2011/1617). This work formed part of the APACA III project, financially supported by the European Union (ERDF), the French Ministry of Industry (DIRECCTE), and the Midi-Pyrénées Region.

ORCID

Laurent Arurault  <https://orcid.org/0000-0003-2364-2236>

REFERENCES

- Ozkan S, Mazare A, Schmuki P. Critical parameters and factors in the formation of spaced TiO₂ nanotubes by self-organizing anodization. *Electrochim Acta*. 2018;268:435-447.
- Toccafondi C, Stepniowski WJ, Leoncini M, Salerno M. Advanced morphological analysis of patterns of thin anodic porous alumina. *Mater Charact*. 2014;94:26-36.
- Habazaki H, Oikawa Y, Fushimi K, et al. Importance of water content in formation of porous anodic niobium oxide films in hot phosphate-glycerol electrolyte. *Electrochim Acta*. 2009;54(3):946-951.
- Chen W, Tu Q, Wu H, et al. Study on morphology evolution of anodic tantalum oxide films in different using stages of H₂SO₄/HF electrolyte. *Electrochim Acta*. 2017;236:140-153.
- Shin H-C, Dong J, Liu M. Porous tin oxides prepared using an anodic oxidation process. *Adv Mater*. 2004;16(3):237-240.
- Jang YS, Kim YK, Park IS, et al. Film characteristics of anodic oxidized AZ91D magnesium alloy by applied power. *Surf Interface Anal*. 2009;41(6):524-530.
- Garcia-Garcia FJ, Koroleva EV, Thompson GE, Smith GC. Anodic film formation on binary Al-Mg and Al-Ti alloys in nitric acid. *Surf Interface Anal*. 2010;42(4):258-263.
- Wu G, Yu M, Liu J, Li S, Wu L, Zhang Y. Surface characteristics of anodic oxide films fabricated in acid and neutral electrolytes on Ti-10V-2Fe-3Al alloy. *Surf Interface Anal*. 2013;45(2):661-666.
- Furneaux RC, Rigdy WR, Davidson AP. The formation of controlled-porosity membranes from anodically oxidized aluminium. *Nature*. 1989;337(6203):147-149.
- Masuda H, Fukuda K. Ordered metal nanohole arrays made by a two-step replication of honeycomb structures of anodic alumina. *Science*. 1995;268(5216):1466-1468.
- Lee W, Ji R, Gösele U, Nielsch K. Fast fabrication of long-range ordered porous alumina membranes by hard anodization. *Nat Mater*. 2006;5(9):741-747.
- Lee W, Schwirn K, Steinhart M, Pippel E, Scholz R, Gösele U. Structural engineering of nanoporous anodic aluminium oxide by pulse anodization of aluminium. *Nat Nanotechnol*. 2008;3(4):234-239.
- Le Coz F, Arurault L, Fontorbes S, Vilar V, Datas L, Winterton P. Chemical composition and structural changes of porous templates obtained by anodizing aluminium in phosphoric acid electrolyte. *Surf Interface Anal*. 2010;42(4):227-233.
- Le Coz F, Arurault L, Datas L. Chemical analysis of a single basic cell of porous anodic aluminium oxide templates. *Mater Charact*. 2010;61(3):283-288.
- Saenz de Miera M, Curioni M, Skeldon P, Thompson GE. Preferential anodic oxidation of second-phase constituents during anodising of AA2024-T3 and AA7075-T6 alloys. *Surf Interface Anal*. 2010;42(4):241-246.
- Goueffon Y, Arurault L, Mabru C, Tonon C, Guigues P. Black anodic coatings for space applications: study of the process parameters, characteristics and mechanical properties. *J Mater Process Technol*. 2009;209(11):5145-5151.
- Zhao S, Fan H, Yin N, et al. Image binarization to calculate porosity of porous anodic oxides and derivation of porosity vs current. *Mater Res Bull*. 2017;93:138-143.
- Giffard K, Arurault L, Blanc C. Dynamic measurements and wettability phenomena in mesoporous anodic films prepared on 1050 and 2024T3 aluminium alloys. *Micropor Mesopor Mat*. 2016;235:32-41.
- Priet B, Odemer G, Blanc C, Giffard K, Arurault L. Effect of new sealing treatments on corrosion fatigue lifetime of anodized 2024 aluminium alloy. *Surf Coat Technol*. 2016;307:206-219.
- Van Put MA, Abrahams ST, Elisseeva O, de Kok JMM, Mol JMC, Terryn H. Potentiodynamic anodizing of aluminium alloys in Cr(VI)-free electrolytes. *Surf Interface Anal*. 2016;48:946-952.
- Wilson SJ, Stacey MH. The porosity of aluminium oxide phases derived from well-crystallized boehmite: correlated electron microscope, adsorption, and porosimetry studies. *J Colloid Interface Sci*. 1981;82(2):507-517.
- Cook RA, Hover KC. Mercury porosimetry of cement-based materials and associated correction factors. *Construct Build Mater*. 1993;7(4):231-240.
- Diamond S. Mercury porosimetry: an inappropriate method of the measurement of pore size distributions in cement-based materials. *Cem Concr Res*. 2000;30(10):1517-1525.
- Bessone JB. The activation of aluminium by mercury ions in non-aggressive media. *Corros Sci*. 2006;48(12):4243-4256.
- Moutarlier V, Gigandet MP, Pagetti J, Linget S. Influence of molybdate species added to sulphuric acid on composition and morphology of the anodic layers formed on 2024 aluminium alloy. *Thin Solid Films*. 2005;483(1-2):197-204.
- Dekker AJ, Van Geel WC. On the amorphous and crystalline oxide layer of aluminium. *Philips Res Rep*. 1947;2:313.
- Dekker A, Middelhoek A. Transport number and the structure of porous anodic films on aluminium. *J Electrochem Soc*. 1970;117(4):440-448.
- Takahashi H, Nagayama M. The determination of the porosity of anodic oxide films on aluminium by the pore-filling method. *Corros Sci*. 1978;18(10):911-925.
- Lemaitre L, Franssaer J, Van Peteghem AP, Moors M, Wettinck E. The application of the pore-filling method to the study of the structure of porous anodic films on aluminium. *Mater Chem Phys*. 1987;17(3):285-291.
- Debuyck F, Moors M, Van Peteghem AP. The influence of the anodization temperature and voltage on the porosity of the anodization layer on aluminium. *Mater Chem Phys*. 1993;36(1-2):146-149.
- Ono S, Masuko N. Dissolution behavior of the barrier layer of porous anodic films formed on aluminium studied by pore-filling technique. *J Light Metal Soc Japan*. 1993;43(9):447-452.
- Ono S, Masuko N. Evaluation of pore diameter of anodic porous films formed on aluminium. *Surf Coat Technol*. 2003;169 - 170:139-142.
- Machkova M, Girginov A, Klein E, Ikonopisov S. Breakdown phenomena during the pore-filling of anodic oxide films on aluminium. *Surf Technol*. 1981;14(3):241-244.

34. Machkova M, Klein E, Girginov A, Ikonopisov S. Pore filling and attendant breakdown of thick anodic films on aluminium. *Surf Technol.* 1984;22(1):21-28.
35. Ikonopisov S, Girginov A, Machkova M. Galvanoluminescence during the pore filling of anodic films on aluminium formed in sulfuric acid. *Electrochim Acta.* 1989;34(5):631-634.
36. Girginov A, Machkova M, Ikonopisov S. Light emission during the pore-filling of anodic alumina films with strong own galvanoluminescence. *Electrochim Acta.* 1990;35(5):825-826.
37. Girginov A, Zahariev A, Machkova M. Kinetics of formation of complex anodic films on aluminium. *Mater Chem Phys.* 2002;76(3):274-278.
38. Girginov A, Zahariev A, Klein E. Electronic conductivity of the (+)aluminium/complex anodic film/electrolyte system. *J Mater Sci Mater Electron.* 2002;13:543-548.
39. Zahariev A, Girginov A. Formation of complex anodic films on porous alumina matrices. *Bul Mater Sci* 2003. 2003;26(3):349.
40. Girginov C, Zahariev A, Kanazirski I. Breakdown phenomena during the formation of complex anodic films on aluminium. *C R Acad Bulg Sci.* 2011;64:1117-1122.
41. Petukhov DI, Napolskii KS, Eliseev AA. Permeability of anodic alumina membranes with branched channels *Nanotechnology* 2012;23, 335601 (6pp).
42. Grigor'ev SV, Grigor'eva NA, Syromyatnikov AV, et al. Two-dimensional spatially ordered Al₂O₃ systems: small-angle neutron scattering investigation. *JETP Letters.* 2007;85(9):449-453.

How to cite this article: Giffard K, Arurault L, Blanc C, Di Caprio D. Accurate evaluations of both porosity and tortuosity of anodic films grown on rolled AA 1050 and on rolled or machined AA 2024 T3. *Surf Interface Anal.* 2018;1-10. <https://doi.org/10.1002/sia.6606>